

MPS-DEM Method for Particle Effects on Mixed Transportation Characteristics of Horizontal Pipeline

Xuanjing Pan¹, Zhiyuan Wei², Decheng Wan^{1*}

¹Computational Marine Hydrodynamics Lab (CMHL), School of Naval Architecture, Ocean and Civil Engineering,
Shanghai Jiao Tong University, Shanghai, China

²Marine Design & Research Institute of China, Shanghai, China

*Corresponding author

ABSTRACT

In recent years, with the development of ship and ocean engineering to the deep sea, people pay more and more attention to the ore mining and transportation in the deep sea. Deep sea mineral transportation involves horizontal pipeline transportation. The horizontal pipeline has the characteristics of large slenderness ratio and high liquid velocity. Considering the complexity of this problem and the problem of solid-liquid two-phase flow, this paper intends to study this problem by using the combination of moving particle semi implicit method (MPS) and discrete element method (DEM). It is a new attempt to use MPS method to simulate liquid flow in pipeline, and DEM method is a particle numerical method based on discontinuous medium assumption, which is especially suitable for solving solid particles in mixed transportation by averaging ore shape with spherically shaped solid particles.

The process and details of mixed transportation in ultra long horizontal pipeline are not clear. In this paper, periodic boundary conditions are used to splice multiple sections of pipes to form an ultra long horizontal pipeline. Based on the MPSDEM-SJTU solver independently developed by our research group, the particle motion state and flow field information under different solid particle concentration conditions are analyzed. These results are expected to provide reference for setting transportation parameters and optimizing transportation conditions.

KEY WORDS: Ultra long horizontal pipeline, Solid liquid mixed transportation, MPS method, DEM method, Particle concentration.

INTRODUCTION

In recent years, the mining of marine ore has gradually attracted people's attention. Chung et al. (2021) made some summary work on deep-sea mining. Generally speaking, the length of the horizontal pipeline is very large so that the liquid-solid two-phase flow problem involved is very complicated. Oh J, Jung J (2015, 2018) did series work. What's more, when the liquid flow rate in the pipeline is small, it will cause the solid particles to accumulate and block in the pipeline, so the liquid flow rate in the horizontal pipeline is generally set to be large. Miedema SA (2015) have done research in this area. Senapati PK, Mishra

BK, Parida A (2013) found that after full development, the Reynolds number in the pipeline is very large, which will generate a lot of large turbulence, moreover, the shape, quantity and position of the solid particles are uncertain, there will be many difficulties in analyzing the problem.

Generally speaking, for the problem of liquid-solid two-phase flow in ultra-long pipelines, the experimental method is expensive and costly, which is generally not used. However, the method of numerical simulation has high repeatability and low cost, and it is generally used for research. The shapes of marine ores are different. In order to highlight the key points of the problem, the spherical shape is considered to represent the average ore shape. The numerical simulations of liquid and solid phases are mainly related by coupling methods. The coupling types are mainly divided into Euler-Euler type by Messa GV, Malavasi S (2015), Euler-Lagrange type by Uzi A, Levy A (2018) and Lagrange-Lagrange type. The Euler-Euler type is also known as the two-fluid type, that is, the Euler method is used to study both liquids and solids. This method is relatively simple to deal with, but the calculation accuracy is not high because it cannot accurately simulate the physical processes such as particle-to-particle collisions; The Euler-Lagrange type is based on the different characteristics of liquids and solids. The Euler method is used to study liquids and the Lagrange method is used to study solids, which can ensure the calculation accuracy of the collision process between particles and particles. The amount of calculation is not too high, so that it is currently the most widely used. Among them, Zhou et al. (2019) conducted a series of parameter studies on the pipe flow problem under this method; The Lagrange-Lagrange type is to use the Lagrange method to study both liquids and solids. This method fully guarantees the accuracy of the solution of liquids and solids, especially in the case of large-scale motion problems. The range of movement is very large, and the computational advantage is reflected. So far, there are almost no precedents for using the Lagrange-Lagrange method to solve the three-dimensional super-long pipe flow problem. For the MPS-DEM approach, only a handful of research teams have done some relevant work. For example, Li et al. (2019) modeled 3D non-Newtonian solid-liquid flow with free surfaces using DEM-MPS, and Harada et al. (2019) performed numerical simulations of the dynamics of beach slope morphology based on a coupled DEM-MPS model. Xie et al.

(2021a,b) has developed the MPS-DEM coupling method and successfully applied the method to the simulation of solid-liquid two-phase flow and fluid-solid coupling problems. This article is going to use this method to study the problem of ultra-long horizontal pipe flow. For the particle motion problem in horizontal pipelines, Uzi et al. (2018) made a series of studies in the flow characteristics of hydraulically conveyed coarse particles, and Zhou et al. (2020) made a series of studies in the fluid model and analysis of hydraulically conveyed coarse particles.

The structure of this article is roughly as follows: Firstly, the governing equations of the liquid and solid phases are given, and the numerical realization of their interaction is given. Then, under the MPS-DEM model, the motion state of the solid particles in the pipeline under different inclination angles, the axial liquid velocity, the particle position distribution and the rotation angular velocity are analyzed. Finally, a series of conclusions on ultra-long pipe flow under different inclination angles are summarized.

METHODOLOGY

Liquid phase

The momentum equation of fluid, also known as the Navier-Stokes equation, is used to describe the momentum exchange between fluids. For the liquid-solid two-phase flow problem, Anderson and Jackson (1969) proposed a local averaging method to balance the momentum equation. In turn, this approach Kafui KD et al. (2002) invented divides the momentum equation into two different models depending on how the pressure term is treated—Model A and Model B. In this paper, Model B will be used to describe the momentum equation of the fluid. Xie et al. (2021a) have used this MPS-DEM model before.

$$\frac{\partial}{\partial t}(\tilde{\rho}_l) + \nabla \cdot (\tilde{\rho}_l \bar{u}) = 0 \quad (1)$$

$$\frac{D}{Dt}(\tilde{\rho}_l \bar{u}) = -\nabla p + \varepsilon_l \mu_l \nabla^2 \bar{u} + \tilde{\rho}_l \bar{g} - \bar{f}_{\text{int}} \quad (2)$$

$$\tilde{\rho}_l = \varepsilon_l \rho_l \quad (3)$$

where the subscript l represents the liquid particles, ρ_l , \bar{u} , p , ε_l , μ_l , \bar{g} and t represent the liquid density, velocity, pressure, local volume fraction, dynamic viscosity, gravitational acceleration, and physical time, respectively. $\tilde{\rho}_l$ represents the density of the liquid after considering the local volume fraction, \bar{f}_{int} represents the interaction force between solid particles and liquid particles.

In the MPS method, the interaction between particles is characterized by a kernel function, generally represented by $W(r)$. In the process of discretizing the fluid equation, the kernel function acts as a weight function. In order to avoid non-physical pressure oscillations, the kernel function model proposed by Zhang et al. (2014) will be used in this paper.

$$W(r) = \begin{cases} \frac{r_e}{0.85r + 0.15r_e} - 1 & 0 \leq r < r_e \\ 0 & r \leq r_e \end{cases} \quad (4)$$

where r represents the distance between two particles, r_e represents the

effective radius of the interaction between the particles. The strength of this interaction decreases with distance.

In addition, the particle number density is used to describe the distribution of particles, which is proportional to the liquid density and is determined by the following formula,

$$\langle n \rangle_i = \sum_{j \neq i} W(|\bar{r}_j - \bar{r}_i|) \quad (5)$$

where n is the particle number density, the subscripts i and j represent two different particles, \bar{r}_i and \bar{r}_j respectively represent its position relative to the origin. For incompressible fluids, the particle number density n is required to be consistent with the initial particle number density n_0 . For liquid-solid two-phase flow, the local volume fraction should be considered and the particle number density should be kept consistent with the initial particle number density.

$$\langle n \rangle_i = \varepsilon_i n_0 = n_0 \quad (6)$$

The models of particle interaction mainly include gradient model, divergence model and Laplace model, as shown in the following formula,

$$\langle \nabla \phi \rangle_i = \frac{d}{n_0} \sum_{j \neq i} \frac{\phi_j + \phi_i}{|\bar{r}_j - \bar{r}_i|^2} (\bar{r}_j - \bar{r}_i) W(|\bar{r}_j - \bar{r}_i|) \quad (7)$$

$$\langle \nabla \cdot \bar{u} \rangle_i = \frac{d}{n_0} \sum_{j \neq i} \frac{(\bar{r}_j - \bar{r}_i) \cdot (\bar{u}_j - \bar{u}_i)}{|\bar{r}_j - \bar{r}_i|^2} W(|\bar{r}_j - \bar{r}_i|) \quad (8)$$

$$\langle \nabla^2 \phi \rangle_i = \frac{2d}{n_0 \lambda} \sum_{j \neq i} (\phi_j - \phi_i) W(|\bar{r}_j - \bar{r}_i|) \quad (9)$$

In the formula, n_0 is replaced by n_0 , ϕ is the physical quantity carried by the liquid particles, d is the spatial dimension. In this paper, the problem solved is three-dimensional pipeline flow, so d is taken as 3.

λ is a parameter that increases the variance to equal to the analytical solution, as shown in the following equation.

$$\lambda = \frac{\sum_{j \neq i} W(|\bar{r}_j - \bar{r}_i|) \cdot |\bar{r}_j - \bar{r}_i|^2}{\sum_{j \neq i} W(|\bar{r}_j - \bar{r}_i|)} \quad (10)$$

The pressure of the flow field is obtained by solving the pressure Poisson equation (PPE). In this paper, the mixed source term method proposed by Tanaka is used to solve the PPE.

$$\nabla^2 p_i^{m+1} = (1 - \gamma) \frac{\rho_l}{\Delta t} \nabla \cdot \bar{u}_i^{*} - \gamma \frac{\rho_l}{\Delta t^2} \frac{\langle n^* \rangle_i - n_0}{n_0} \quad (11)$$

where p_i^{m+1} represents the pressure at the $m+1$ th time step, γ is a blending parameter between 0 and 1, Δt is the time step, \bar{u}_i^{*} and

$\langle n^* \rangle_i$ represent the median velocity and median number density of particles. This article sets the value of γ to 0.001.

Solid phase

The equation of motion of solid particles is based on Newton's second law and the equation of rotation,

$$m_p \frac{D\bar{v}_p}{Dt} = \sum_l \bar{F}_{pq} + m_p \bar{g} + \bar{F}_p^{\text{int}} \quad (12)$$

$$I_p \frac{D\bar{\omega}_p}{Dt} = \sum_l \bar{T}_{pq} \quad (13)$$

In the formula, the subscripts p and q represent two different solid particles. m_p , I_p , \bar{v}_p , $\bar{\omega}_p$ represent the mass, moment of inertia, translational velocity and rotational angular velocity of the solid particle p respectively. \bar{F}_{pq} and \bar{T}_{pq} are the contact force and contact moment between solid particles p and q respectively. \bar{F}_p^{int} represents the sum of the forces acting on the solid particle p by the liquid.

Cundall and Strack (1979) proposed the soft sphere model in the solid particles. The contact model between the soft balls consists of a spring, a damper and a slider, the spring provides stiffness, the damper provides damping, and the slider constitutes the member of the coupling direction of the normal force and the tangential force between the particles.

The contact force \bar{F}_{pq} is divided into two dimensions: normal and tangential. The normal force \bar{F}_{pq}^n is determined by the following formula,

$$\bar{F}_{pq}^n = -k\bar{x}_{pq}^n - c\bar{v}_{pq}^n \quad (14)$$

where \bar{x}_{pq}^n and \bar{v}_{pq}^n represent the relative displacement and velocity of solid particles p and q in the normal direction, respectively. k and c represent the stiffness of the spring and the damping coefficient of the damper, respectively.

The tangential force \bar{F}_{pq}^t is determined by the following formula,

$$\bar{F}_{pq}^t = \begin{cases} -k\bar{x}_{pq}^t - c\bar{v}_{pq}^t & |\bar{F}_{pq}^t| < \mu_s |\bar{F}_{pq}^n| \\ -\mu_s |\bar{F}_{pq}^n| \frac{\bar{x}_{pq}^t}{|\bar{x}_{pq}^t|} & |\bar{F}_{pq}^t| > \mu_s |\bar{F}_{pq}^n| \end{cases} \quad (15)$$

where \bar{x}_{pq}^t and \bar{v}_{pq}^t represent the relative displacement and velocity of solid particles p and q in the tangential direction, respectively. μ_s is the static friction coefficient. When the normal contact force is less than the critical force, there is static friction between solid particles. When the normal contact force is greater than the critical force, there is sliding friction between solid particles.

Two-phase interaction

The forces of liquid acting on solid particles mainly include buoyancy, drag force, lubricating force, etc. Because buoyancy and drag forces dominate, other components are ignored in this paper, and only buoyancy and drag forces are considered. The drag force \bar{F}_p^d adopts the model proposed by Ergun (1952) and Wen-Yu (1966), which is determined by the following formula,

$$\bar{F}_p^d = \frac{\beta_p}{1 - \varepsilon_p} (\bar{u}_p - \bar{v}_p) V_p \quad (16)$$

In the formula, V_p represents the volume of the solid particle p , and \bar{v}_p represents the velocity of the solid particle p . ε_p and \bar{u}_p represent the local volume fraction and central liquid velocity at the solid particle p . \bar{F}_p^d depends on the local volume fraction at the solid particles, the relative velocity between the liquid and the solid. The interface momentum exchange coefficient β_p is determined by the following formula,

$$\beta_p = \begin{cases} 150 \frac{(1 - \varepsilon_p)^2}{\varepsilon_p} \frac{\mu_l}{d_p^2} + 1.75(1 - \varepsilon_p) \frac{\rho_l}{d_p} |\bar{u}_p - \bar{v}_p| & \varepsilon_p \leq 0.8 \\ 0.75 C_d \frac{\varepsilon_p (1 - \varepsilon_p)}{d_p} \rho_l \varepsilon_p^{-2.65} |\bar{u}_p - \bar{v}_p| & \varepsilon_p > 0.8 \end{cases} \quad (17)$$

In the formula, d_p is the diameter of the solid particle p , and C_d is the drag coefficient, which is determined by the following formula,

$$C_d = \begin{cases} \frac{24}{\text{Re}_p} (1 + 0.15 \text{Re}_p^{0.687}) & \text{Re}_p \leq 1000 \\ 0.44 & \text{Re}_p > 1000 \end{cases} \quad (18)$$

The Reynolds number of the solid particle p is determined by,

$$\text{Re}_p = \frac{\varepsilon_p \rho_l d_p |\bar{u}_p - \bar{v}_p|}{\mu_l} \quad (19)$$

An extra weight function used to describe the solid-fluid interaction, written as,

$$W_s(r) = \begin{cases} 4(r/r_e)^5 - 5(r/r_e)^4 + 1 & r < r_e \\ 0 & r \geq r_e \end{cases} \quad (20)$$

The local volume fraction of fluid particle i is calculated as,

$$\varepsilon_i = 1 - \frac{1}{\int W_s(|\bar{r}|) d\bar{r}} \sum_p W_s(|\bar{r}_i - \bar{r}_p|) V_p \quad (21)$$

The local volume fraction and fluid velocity in the position of solid particle p are decided by neighboring fluid particles through the weight function, given by,

$$\varepsilon_i = \frac{\sum_i \varepsilon_i W_s(|\vec{r}_i - \vec{r}_p|)}{\sum_i W_s(|\vec{r}_i - \vec{r}_p|)} \quad (22)$$

The buoyancy and drag force are combined to obtain the total force \vec{F}_p^{int} of the liquid acting on the solid particle p .

The reaction force \vec{f}_i^{int} acting on the liquid particles needs to satisfy Newton's first law and is determined by the following formula,

$$\vec{f}_i^{\text{int}} = \frac{1}{V_i} \sum_p \left(\vec{F}_p^{\text{int}} \frac{W_s(|\vec{r}_i - \vec{r}_p|)}{\sum_j W_s(|\vec{r}_i - \vec{r}_p|)} \right) \quad (23)$$

where V_i represents the volume of liquid particles.

Boundary conditions

Pipe wall

As shown in Fig. 1, there are multiple layers of MPS particles arranged at the boundary of the pipe wall. At the inner wall of the pipe, there is a layer of wall particles, and its pressure is solved by PPE, where the centers of all the wall particles are connected to form the inner wall boundary of the pipe. There are two layers of the ghost particles at the outer wall, which mainly provide support for the fluid particles near the solid wall, whose pressure is obtained by extrapolation. Neither the wall particles nor the ghost particles will update their velocity and displacement after obtaining the pressure.

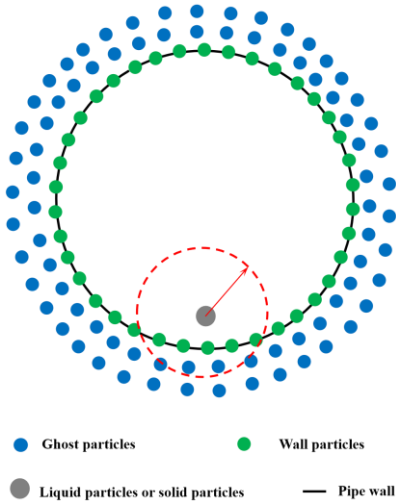
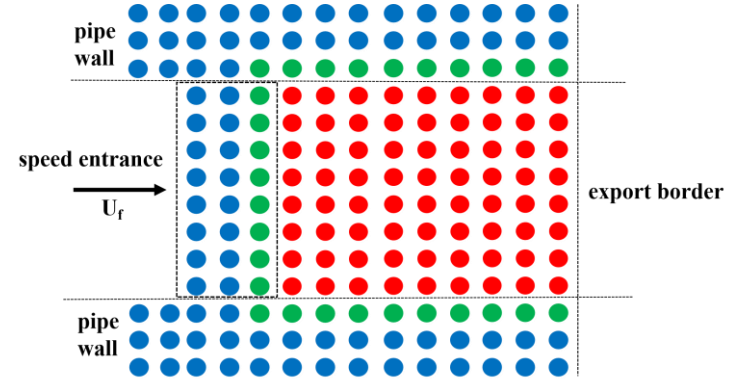


Fig. 1 Schematic diagram of pipe wall boundary

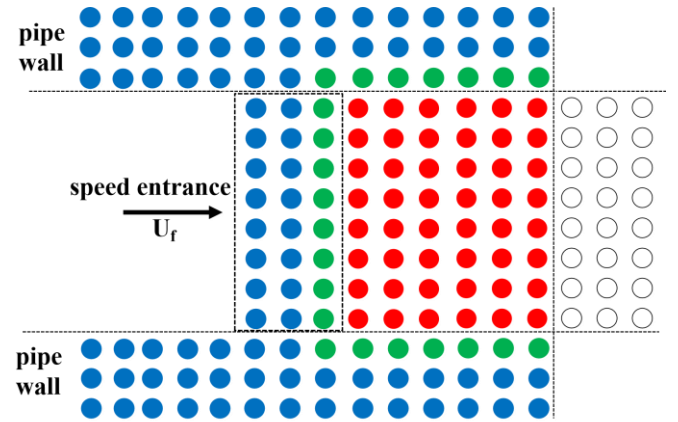
Entrance and exit

In this paper, the pipeline is set with inlet and outlet, and periodic boundary conditions are considered, as shown in Fig. 2. At the initial moment, the push plate at the entrance moves to the right, pushing the

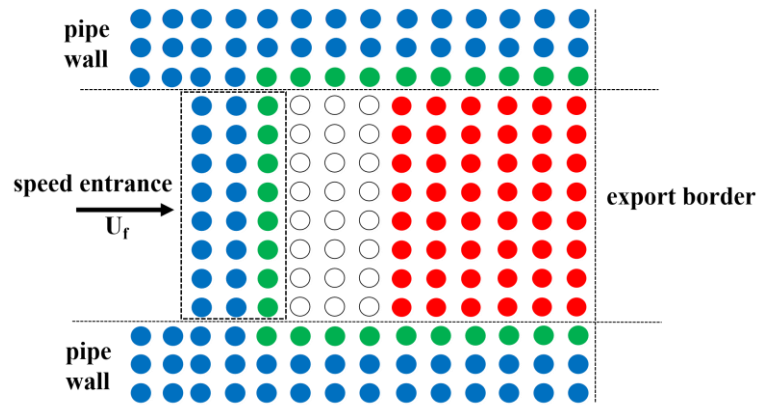
liquid particles to move. When the push plate reaches the set position, it will immediately return to its original position, and the gap will be filled with dummy particles without any physical properties. Physical quantities such as velocity and pressure are then assigned to the dummy particles, turning them into liquid particles. The constant reciprocation of the push plate will push all the liquid particles to the right and drive the solid particles to move at the same time. When liquid and solid particles come out of the outlet, they will re-enter the area from the inlet. Among them, solid particles will inherit the physical information of the previous time step (including velocity, pressure, etc.), while liquid particles will not inherit. Therefore, the calculation can continue.



(a) Initial state



(b) The push plate moves to the right to the specified position



(c) The push plate returns to the initial position

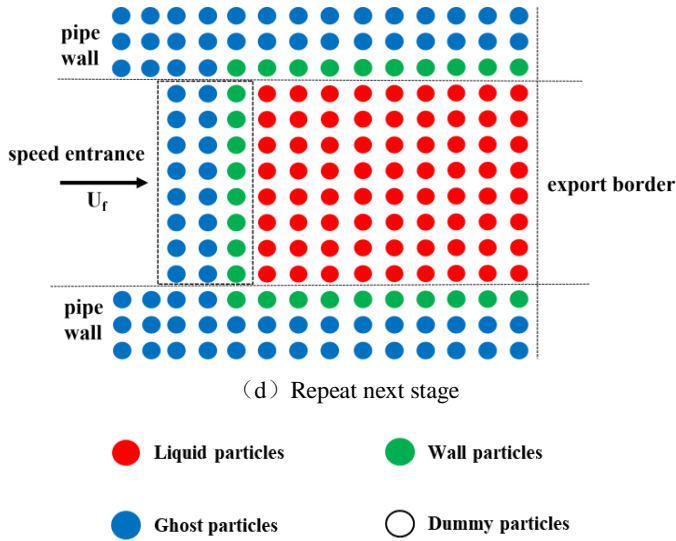


Fig. 2 Schematic diagram of entrance and exit boundary

Time Step

The MPS method for incompressible fluids is a semi-implicit method, while the DEM method is an explicit method. The time step of DEM is generally much smaller than that of MPS. For the stability of the simulation, the MPS-DEM coupling method studied by the predecessors generally chooses a small time step, which takes a long time. In this paper, a multi-time-step algorithm is introduced for these two methods. The time step of MPS satisfies the Courant-Friedrichs-Lewy (CFL) condition and is determined by the following equation,

$$\frac{u_{l,max} \Delta t_{mps}}{\Delta l_0} < C \quad (24)$$

where $u_{l,max}$, Δt_{mps} , Δl_0 and C represent the maximum velocity of the liquid particles, the time step, the initial particle spacing and the Courant number, respectively.

The time step of the DEM is determined by,

$$\Delta t_{dem} < \frac{\pi R \sqrt{\rho / G}}{0.0163\nu + 0.8766} \quad (25)$$

In this paper, the time step of MPS is set to 10^{-4} s, and the time step of DEM is set to 10^{-6} s.

NUMERICAL MODELS

Fig. 3 shows the distribution of MPS particles and DEM particles at the initial moment. The number of MPS particles is 324246, the particle radius is 0.005 m (where Type=-2 is the wall particles, Type=-1 is the ghost particles, and Type=2 is the liquid particles). The number of DEM particles is $8 \times 8 \times 8$, and the initial moment is set as a cubic arrangement. The transport speed is set to 1m/s, and the results of each physical quantity from the initial moment (0s) to the full development (34s) are compared.

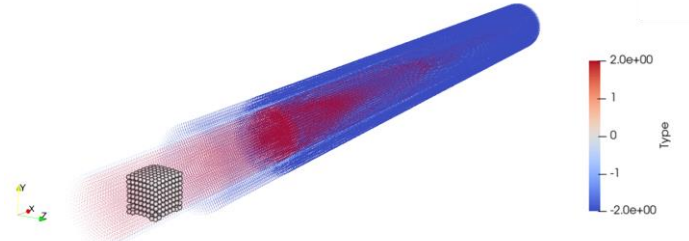


Fig. 3 MPS and DEM models

The pipes used in this numerical simulation are horizontal pipes. The solid particles are initially distributed at the entrance of the pipeline. The drag force of the liquid drives the solid particles to move forward along the pipeline. Assuming that the upward direction of the length of the pipe is the positive x-axis, we set the direction of the gravitational acceleration along the radial direction of the pipe (positive y-axis), the size is -9.807 m/s^2 , the length of the pipe is 4 m, and the radius is 0.1 m, as shown in Fig. 4.



Fig. 4 Pipeline model

The detailed parameters of the liquid and solid particles are shown in Table 1. When the liquid flow rate is equal to 1 m/s, according to

publicity $R_e = \frac{\rho_l v D}{\mu_l}$, it can be calculated that the overall flow in the

pipe $R_e = 200000$. At this time, the flow in the pipe is in the form of turbulence, and the liquid velocity is relatively flat along the radial distribution of the pipe.

Table 1. Detailed parameters of liquids and solids

| Liquid phase | Unit | Numerical value |
|--------------------------|-------------------|----------------------|
| Density | kg/m ³ | 1000 |
| Kinematic viscosity | m ² /s | 1.0×10^{-6} |
| Initial particle spacing | m | 0.0075 |
| Time step | s | 1.0×10^{-4} |
| Solid phase | Unit | Numerical value |
| Density | kg/m ³ | 2700 |
| Radius | m | 0.01 |
| Young's modulus | N/m ² | 1.0×10^8 |
| Poisson's ratio | / | 0.2 |
| Friction coefficient | / | 0.2 |
| Restitution coefficient | / | 0.9 |
| Time step | s | 1.0×10^{-6} |

NUMERICAL RESULTS

From the initial moment (0 s), the solid particles are arranged in a cubic

form. After that, due to the drag force of the liquid, the solid particles move forward continuously until the 34th s, the solid particles flow out from the outlet of the pipe, and return to the inlet to reciprocate according to the physical process shown in Fig. 2. For this stage from the static state to the fully developed state, it is necessary to analyze its physical laws and mechanical properties. The time history process from 0 s to 34 s is arranged as shown in Fig. 5.

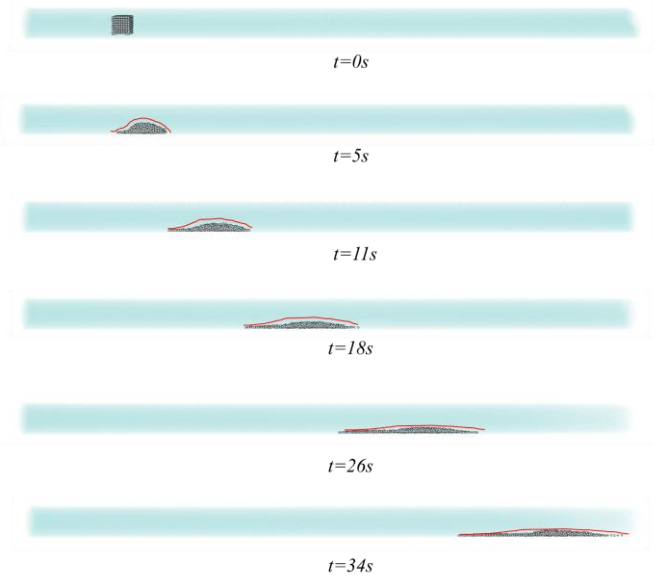


Fig. 5 Time course of solid particles

Among them, it can be seen that the overall outline of the solid particles (indicated by red line) presents a shape with low ends at both ends and high in the middle. From start to finish, this profile is continuously elongated and tends to fill the entire pipe. During the movement, the overall shape of the contour remains low at both ends and high in the middle. The reason is to minimize the movement resistance during the movement, so as to reduce the energy loss.

In addition, take $t=0$ s, $t=5$ s, $t=11$ s and $t=18$ s to analyze the velocity of solid particles, as shown in Figure 6. Among them, the color band is 0-1 m/s, the color is dark blue when the speed is 0, and the color is dark red when the speed is 1. It can be seen that at $t=0$ s, the color of all solid particles is dark blue, reflecting that all solid particles are in a static state at this time; at $t=5$ s, the solid particles begin to collapse, and the solid particles still maintain a relatively compact outline because they are not fully developed at this time; at $t=11$ s, the solid particles are gradually flattened due to the drag force of the liquid. It can also be seen more clearly from the color map that the color of the particles located at the front end of the particle cluster is red, the color of the particles located at the rear end of the particle cluster is blue, the color of the particles located in the upper part of the particle cluster is red, and the color of the particles located in the upper part of the particle cluster is red. The color of particles in the lower part of the cluster is blue, which reflects that the velocity distribution of particle motion is characterized by a large front end, a small rear end, a large upper part and a small lower part. At $t=18$ s, the solid particles are continued to be flattened to the entire pipeline, and the velocity distribution characteristics are similar to those before.

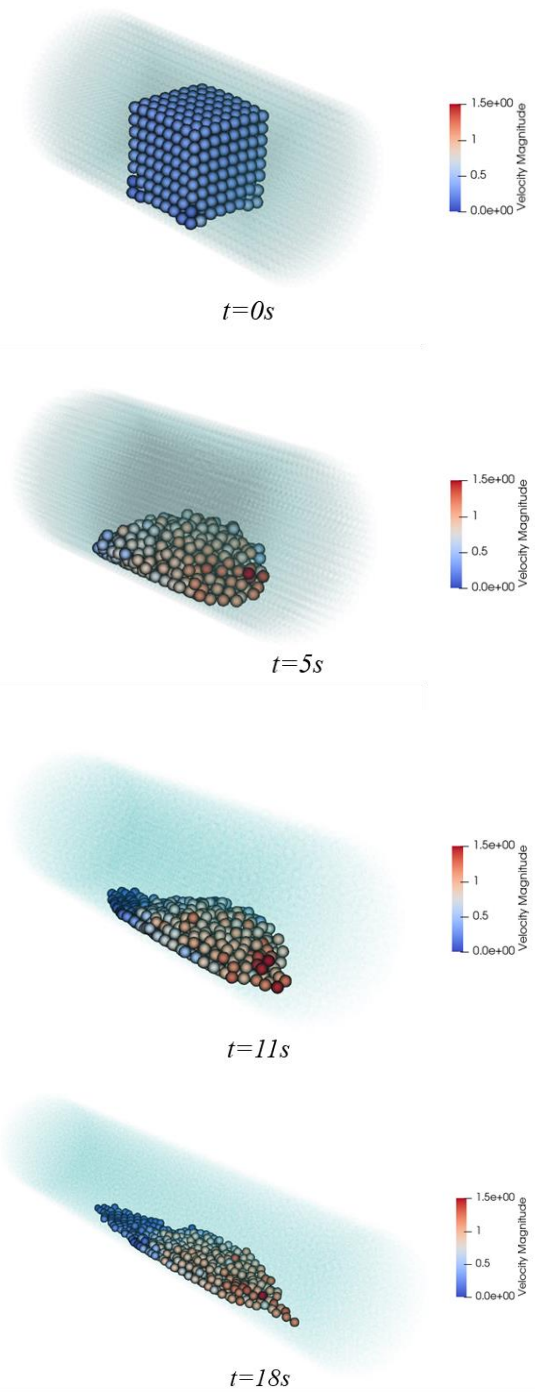


Fig. 6 The collapse process of solid particles

As shown in Fig. 7, at $t=2$ s, we cut a cross-section in the middle of the solid particle cluster and analyze the velocity distribution of this cross-section.

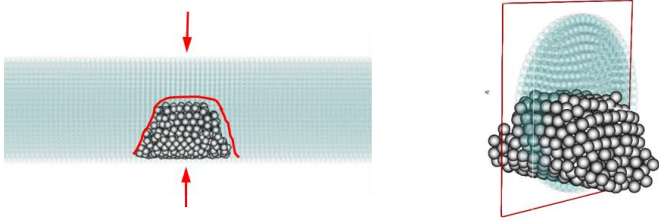


Fig. 7 Cross-sectional view at 2s

As shown in Fig. 8, the rough outline of the solid particles is outlined with red lines. Reflected in the velocity cloud map, the color band of the velocity is 0-1 m/s, the color is dark blue when the speed is 0, and the color is dark red when the speed is 1m/s. The contours outlined with this red line are reflected indiscriminately on the velocity contour. The region with a solid particle velocity of 0.5 m/s is located approximately in the middle of the solid particle cluster. This illustrates the applicability of velocity contours.

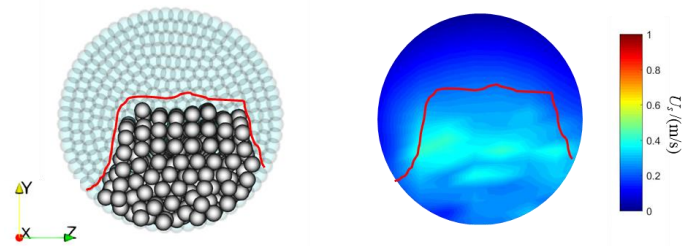


Fig. 8 Speed cloud map at 2 s

As shown in Fig. 9, at $t=5$ s, we cut a cross-section in the middle of the solid particle cluster and analyzed the velocity distribution of this cross-section.

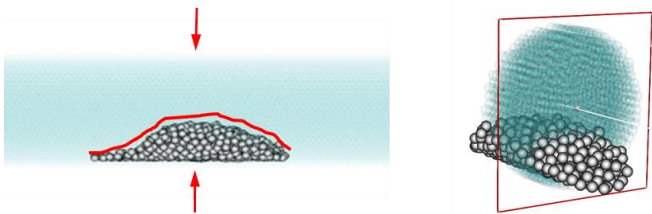


Fig. 9 Cross-sectional view at 5 s

As shown in Fig. 10, the outline of the solid particles is outlined with a red line, which is reflected in the velocity nephogram. It can be seen that the most obvious place for the velocity value is the location of the solid particles. Among them, the position with the redder color is the position of the particle with the larger velocity value, and these positions are mainly distributed in the upper part of the particle cluster. The average speed can reach 1 m/s. While the position with the bluer color is the position of the particle with the smaller velocity value, and these positions are mainly distributed in the particle cluster. The average speed is around 0.5 m/s. The above conclusion is consistent with the previous analysis conclusion.

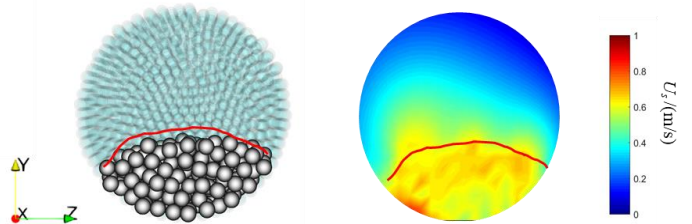


Fig. 10 Speed cloud map at 5 s

CONCLUSIONS

From rest to full development, solid particles move forward continuously. During the movement, the overall contour of the solid particles presents a shape with low ends and high in the middle, and as time goes by, this contour is continuously elongated and tends to cover the entire pipeline. The shape of the solid particles in the movement process is to control the minimum movement resistance during the movement process, so as to reduce the energy loss. And the velocity distribution of solid particle clusters in the movement process is characterized by a large front end, a small rear end, a large upper part and a small lower part.

In the future, for horizontal pipelines, it is also possible to digitally analyze the influence of liquid flow rate, particle size and particle concentration on the flow field in the pipeline.

ACKNOWLEDGEMENTS

This work was supported by the National Natural Science Foundation of China (51879159, 52131102), and the National Key Research and Development Program of China (2019YFB1704200), to which the authors are most grateful.

REFERENCES

- Anderson T.B., Jackson R. (1969). *Fluid mechanical description of fluidized beds. Comparison of theory and experiment*, I & Eng. Chem. Fund, 6(1): 137-144.
- Chung Jin S. (2021). *Manganese Nodule Miners on 18,000-ft Deep Seabed: Touchdown, Track-keeping Control and Disturbed Seabed Track History*, Int. J. Offshore Polar Eng, 31: 385-394.
- Cundall P.A., Strack O.D. (1979). *A discrete numerical model for granular assemblies*, Geotechnolgy, 29(1): 47-65.
- Ergun S (1952). *Fluid flow through packed columns*, Journal of Materials Science and Chemical Engineering, 48(2): 89-94.
- Harada, Ikari, Khayyer, Gotoh (2019). *Numerical simulation for swash morphodynamics by DEM-MPS coupling model*. Coastal Engineering Journal, 61(1): 2-14.
- Kafui KD, Thornton C, Adams MJ (2002). *Discrete particle-continuum fluid modelling for gas-solid fluidized beds*, Chem. Eng. Sci., 57(13): 2395-2410.
- Li JJ, Qiu LC, Tian L, Yang YS, Han Y(2019). *Modeling 3D non-newtonian solid-liquid flows with a free-surface using DEM-MPS*. Engineering Analysis with Boundary Elements, 105(8), 70-77.
- Messa GV, Malavasi S (2015). *Improvements in the numerical prediction of fully suspended slurry flow in horizontal pipes*, Powder Technology, 270: 358-367.
- Miedema SA (2015). *A head loss model for homogeneous slurry transport for medium sized particles*, Journal of Hydrology and Hydromechanics, 63(1): 1-12.
- Oh J, Jung J, Kim H, Hong S, Sung K, Bae D (2015). *Gap size effect on the tribological characteristics of the roller for deep-sea mining robot*,

- Marine Georesources & Geotechnology, 35(1): 120-126.
- Oh J, Jung J, Hong S (2018). On-board measurement methodology for the liquid-solid slurry production of deep-seabed mining, *Ocean Engineering*, 149: 170-182.
- Senapati PK, Mishra BK, Parida A (2013). Analysis of friction mechanism and homogeneity of suspended load for high concentration fly ash & bottom ash mixture slurry using rheological and pipeline experimental data, *Powder Technology*, 250: 154-163.
- Uzi Avi, Levy. (2018). Flow characteristics of coarse particles in horizontal hydraulic conveying, *Powder Technol*, 326: 302-321.
- Wen C, Yu Y (1966). *Chemical Engineering Progress Symposium Series*, Mechanics of fluidization, 62: 100-111.
- Xie F, Zhao W, Wan D (2021a), *Numerical simulations of liquid-solid flows with free surface by coupling IMPS and DEM*, *Apply Ocean Research*, 114: 102771.
- Xie F, Zhao W, Wan D (2021b), *MPS-DEM coupling method for interaction between fluid and thin elastic structures*, *Ocean Engineering*, 236: 109449.
- Zhang Y, Wan D, Hino T (2014). *Comparative study of MPS method and level-set method for sloshing flows*, *Journal of Hydrodynamics*, 26(4): 577-585.
- Zhou M, Wang S, Kuang S (2019). CFD-DEM modelling of hydraulic conveying of solid particles in a vertical pipe, *Powder Technology*, 354: 893-905.
- Zhou M, Wang S, Kun L (2020). *Modeling and analysis of flow regimes in hydraulic conveying of coarse particles*, *Powder Technology*, 373: 543-554.